

Assessment of the Solidification Cracking Susceptibility of Welding Consumables in the Varestraint Test by Means of an Extended Evaluation Methodology

Arne Kromm,* Maximilian Thomas, Thomas Kannengiesser, Jens Gibmeier, and Florian Vollert

Various test methods are available for assessing the susceptibility of materials to solidification cracking during welding. In the widely used Varestraint test, the crack length is selected as a criterion as a function of the applied bending strain. Unfortunately, the crack length does not characterize the material behavior alone but depends to varying degrees on the individual test parameters used, which makes the interpretation of the results difficult. In addition, the crack length is not comparable under different test conditions. To overcome these disadvantages, we have developed a novel evaluation methodology that decouples the machine influence from the material behavior. The measured crack length is related to the maximum possible value specified by welding speed and deformation time. This relative crack length is calculated numerically, considering the orientation of the cracks. Experiments on two high-alloy martensitic welding consumables show that, in contrast to the conventional evaluation, a comparison of different welding parameters becomes possible. Furthermore, the strain rate proved to be a suitable crack criterion in agreement with Prokhorov's hot cracking model.

solidification cracks, liquation cracks and ductility dip cracks (DDC).^[1,2] The present work deals exclusively with solidification cracks.

Most aluminum alloys, high-alloy steels, and almost all nickel-based alloys exhibit a pronounced tendency to solidification cracking. This is particularly related to the face-centered cubic lattice type, which favors the formation of low-melting phases due to slow diffusion rates and low solubility for alloying elements. The high thermal expansion combined with low thermal conductivity also promotes solidification cracking.^[3] In addition to metallurgical influences, design factors, as well as welding parameters, also have an effect on solidification crack initiation, so that their cause can be traced back to the coincident occurrence of metallurgical and thermomechanical effects, which must

be taken into account for an evaluation of the solidification cracking susceptibility.^[4]

1. Introduction


The prevention of hot cracks during the processing of high-alloy materials represents an essential prerequisite for the safety of welded, cast and increasingly additively manufactured components. Hot cracks are intergranular material separations that occur during cooling at the liquid/solid transition, often referred to as the mushy zone. Hot cracks can be subdivided into

1.1. Solidification Cracking Theories

On the phenomenon of solidification cracking, numerous theories and models have been developed.^[5] Examples are the strain theory,^[6] the generalized theory,^[7] its modification^[8,9] or the Rappaz-Drezet-Gremaud (RDG) theory.^[10] However, due to their complexity and the necessary physical parameters most models are only suitable to a limited extent for the practical prediction of the solidification cracking susceptibility. In addition to the physical parameters acting during solidification, the existing microstructure is often difficult to assess experimentally and can lead to misinterpretations.^[11] Kou recently presented a new criterion for predicting solidification as well as liquation cracking susceptibility based on the relationship of temperature and the fraction of solid, which can be calculated by thermodynamic software.^[12–14] The machine learning approach can also be used to estimate the cracking behavior of alloys based on a broad database of Varestraint test results. Zhang et al. demonstrated this for varying welding parameters, strain levels and changing chemical compositions using more than 480 data sets. The models generated show good agreement with the experimentally obtained crack lengths.^[15] Such tools may be used in the future

A. Kromm, M. Thomas, T. Kannengiesser
Division 9.4 Weld Mechanics
Bundesanstalt für Materialforschung und -prüfung (BAM)
Unter den Eichen 87, 12205 Berlin, Germany
E-mail: arne.kromm@bam.de

J. Gibmeier, F. Vollert
Institute for Applied Materials (IAM-WK)
Karlsruhe Institute of Technology (KIT)
Engelbert-Arnold-Straße 4, 76131 Karlsruhe, Germany

 The ORCID identification number(s) for the author(s) of this article can be found under <https://doi.org/10.1002/adem.202101650>.

© 2022 The Authors. Advanced Engineering Materials published by Wiley-VCH GmbH. This is an open access article under the terms of the Creative Commons Attribution License, which permits use, distribution and reproduction in any medium, provided the original work is properly cited.

DOI: 10.1002/adem.202101650

as a robust and inexpensive assistance in estimating the cracking susceptibility. Nevertheless, the testing of materials with regard to solidification cracking remains indispensable. Of great importance here is the Technological Strength Theory of Prokhorov.^[16] It is limited to the phenomenological observation of solidification cracking, without making any qualitative statements about its metallurgical causes or the underlying mechanisms. Instead, the existence of a Brittleness Temperature Range (BTR) is postulated, within which solidification cracking can occur when a critical load (Technological Strength) is exceeded. The Technological Strength Theory represents a comparatively simple but at the same time elegant approach, since solidification cracking is characterized on the basis of only a few experimentally accessible variables.

As shown schematically in **Figure 1** an alloy passes through the BTR during cooling. The upper limit of the BTR is below the liquidus temperature, where the coalescence of the crystallites begins, and the circulation of the melt is increasingly impeded. Prokhorov defines the lower limit of the BTR at a temperature below solidus when the grain boundaries can transfer mechanical stresses between the crystallites. The deformations (strains) leading to solidification cracks are caused by the thermal shrinkage of the solid material during cooling and the volume shrinkage of the melt during the liquid/solid phase transition. Strains can be superimposed also by mechanical stresses during welding. A strain exceeding the ductility limit within the BTR leads to solidification cracking. The strain is assumed to increase linearly with temperature, which also allows a critical temperature-dependent strain rate $d\varepsilon/dT$ to be formulated (Equation (1)). This critical strain rate for temperature drop (CST) can thus be influenced either mechanically or by the temperature control.^[17]

$$\frac{d\varepsilon}{dT} = \frac{\frac{d\varepsilon}{dT}}{\frac{dT}{dt}} \quad (1)$$

The assumed shape of the BTR and the existence of critical strains for crack initiation were proven in experimental investigations by various research groups.^[17–21] While the BTR was originally thought as a material related measure, it is significantly

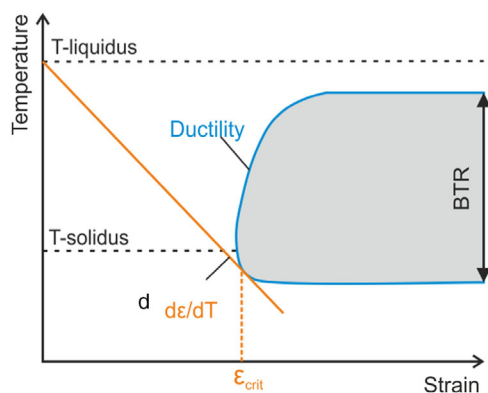


Figure 1. Schematic representation of the Brittleness Temperature Range (BTR) according to Prokhorov et al. and Senda et al.^[16,17] Solidification cracks are formed if a strain (ε_{crit}) exceeds the ductility of the material during cooling.

influenced by the welding parameters in some cases.^[22] Investigations by Nakata et al. and Matsuda et al. have shown, that using slow bending Vrestraint tests, the critical strain for crack initiation ε_{crit} is a function of the strain rate applied.^[20,23] Higher strain rates (Bending speed) showed lower critical strains. Thus, the strain rate can be valid criterion suggesting a strain rate dependent mechanism for solidification cracking.^[22]

1.2. Testing the Solidification Cracking Susceptibility

Due to the complex nature of solidification cracking, the current state of the art does not allow reliable prediction of the occurrence of solidification cracks based on nominal material properties or other boundary conditions. Therefore, experimental tests are necessary.^[24] A whole range of test methods exist for this purpose which basically have in common that they induce a loading condition that provokes the crack formation according to Prokhorov's approach of the Technological Strength. Various welding procedures can be used to subject the materials to appropriately critical temperatures. The second prerequisite, the achievement of a critical strain or strain rate, can be ensured either by so-called self-restraint or by external loading of the specimens.^[25,26]

The local strains in the vicinity of the weld pool can only be recorded with considerable effort, e. g. using digital image correlation (DIC).^[18,27–30] Therefore, mostly the “global” augmented strain is used as a simplified parameter for externally loaded hot crack tests. Some test methods instead consider a critical strain rate as a measure of the hot cracking susceptibility. Examples are the Programmed Deformation Rate test (PVR), the Variable Deformation Rate test (VDR) or the Transverse Motion Weldability (TWM) test.^[31–33]

Generally, the characteristics of the different test methods are always reflected to a certain degree in the cracks produced. Therefore, results from different test methods of a material can only be compared with each other to a limited extent. In the present work, the Vrestraint test principle is used to show how the influence of the test equipment on the result can be considered. The originally contradictory test results then become interpretable and represent material-dependent characteristic values. Before the new evaluation method is introduced the conventional procedure is discussed.

2. Vrestraint Test and Evaluation Procedure

The original Vrestraint test (acronym for “Variable Restraint”) was developed by Savage and Lundin.^[34] The basic principle of the method is the bending deformation of a specimen during welding. In those areas of the weld whose temperature during deformation is in the critical range, the formation of hot cracks is thus forced.

The differences in the design of various testing machines and the test procedures make standardization of the Vrestraint test difficult.^[35,36] Basic descriptions of the procedure can be found in the American Welding Society (AWS) national standard AWS B4.0:2016 and in ISO/TR 17 641-3.^[26,37] Nevertheless, neither document describes the test procedure in sufficient detail to make the results comparable.

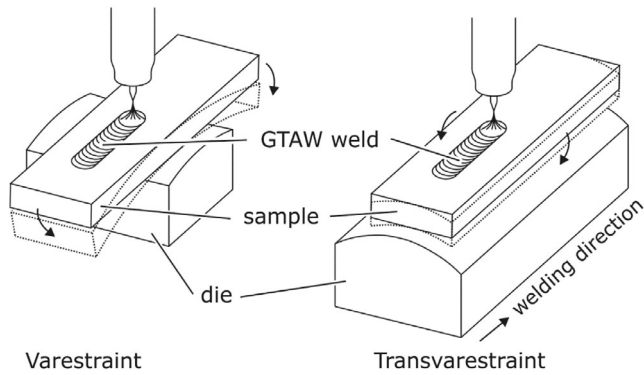


Figure 2. MVT test principles Varestraint and Transvarestraint. Reproduced under terms of the CC-BY license.^[35] Copyright 2020, The Authors, published by Springer Nature.

The adaptation of the Varestraint test used at BAM is the Modified Varestraint/Transvarestraint Test (MVT) developed by Wilken and Kleistner.^[38] Cuboid specimens with fixed dimensions of $100 \times 40 \times 10 \text{ mm}^3$ are used. They are surface melted with a GTAW torch. After half the torch travel the specimen is bent to a defined radius by various combinations of suitable punches and dies.

Within the MVT system the specimens can be bent not only longitudinally to the welding direction, as in the original Varestraint test, but also transversely. This mode is called Transvarestraint (“Transverse Varestraint”). A schematic representation of both modes can be seen in **Figure 2**.

Strains of 1%, 2% or 4% can be augmented in both Varestraint and Transvarestraint modes. The bending speed can be continuously adjusted up to 20 mm s^{-1} . The time taken to reach the full nominal strain is referred to as the deformation time t_{def} . From the augmented strain ϵ the strain rate $\dot{\epsilon}$ can be calculated then after Equation (2).

$$\dot{\epsilon} = \frac{\epsilon}{t_{\text{def}}} \quad (2)$$

2.1. Evaluation of the Cracking Susceptibility

The conventional evaluation of the MVT specimens is carried out according to ISO/TR 17 641-3 by measuring the surface crack lengths formed with the aid of a light microscope at $25\times$ magnification.^[26] The result for each specimen is the total crack length TCL as the sum of the lengths of all cracks, Equation (3). **Figure 3** exemplarily shows cracks found on the surface of a specimen after Varestraint test with an augmented strain of 4%. For reasons of clarity small cracks are not marked in **Figure 3**.

$$\text{TCL} = \sum_{i=1}^n L_n \quad (3)$$

The cracking susceptibility is then quantified by the amount of TCL as a function of the augmented strain and ranked into three categories. In addition to the augmented strain, heat input,

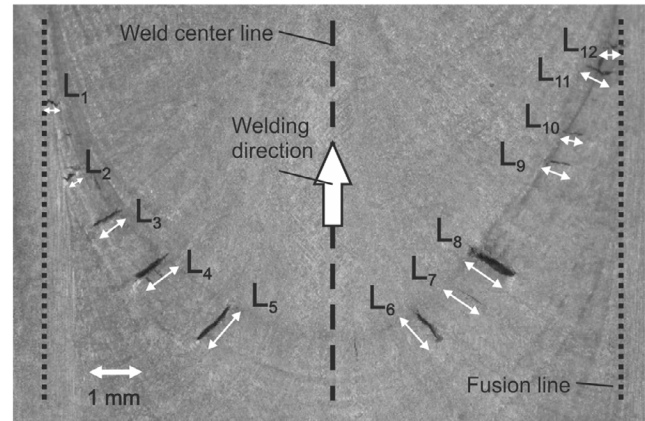


Figure 3. Solidification cracks and its lengths L_n in the weld metal on the surface of a specimen after MVT testing (top view), martensitic filler material, 4% bending strain, not all cracks are marked for reasons of clarity.

welding speed and deformation (strain) rate represent the decisive parameters of Varestraint testing.^[5,36] There is not always agreement in the literature about their respective influence on the extend of cracking, and the selection and evaluation of suitable parameters is still a subject of current research.^[39–42]

One disadvantage of the evaluation based on crack lengths is that the TCL cannot be used 1:1 as a measure of the solidification cracking susceptibility. This is because the location of the cracks around the melt pool is not considered, even though the width of the crack-critical zone is not constant. While the lowest temperature gradient is present in the center of the weld, the isotherms and thus the crack-critical mushy zone are much narrower near the fusion lines. It follows, that short cracks near the fusion lines are equivalent in the sense of cracking susceptibility to long cracks formed in the center of the weld metal, since they represent the same temperature range (BTR). This is already apparent from the exemplary crack lengths shown in **Figure 3**. In the conventional evaluation, this is not considered, i.e. the same material with short off-center cracks would be evaluated better than with long center cracks.

A second disadvantage of the evaluation using TCL is that the cracks grow the longer the loading continues. That is, slow bending leads to longer durations of loading, even if the maximum applied strain is the same. The effect additionally interacts with the welding speed, which determines the distance over which the crack-critical mushy zone or BTR is traveled during stressing.

Both aspects can thus lead to results or apparent trends that are difficult to interpret. The new approach described in the following offers the possibility of taking into account the location of crack initiation as well as the stress duration when evaluating the results.

3. New Evaluation of the Cracking Susceptibility

In contrast to the conventional evaluation, the new methodology is based on the consideration of relative proportions of crack lengths. The crack length L is composed of a material-specific portion d_{BTR} according to the theory of BTR following Prokhorov and a portion d_{def} resulting from the duration of loading (Equation (4)) which causes the crack to propagate.

$$L = d_{\text{BTR}} + d_{\text{def}} \quad (4)$$

In order to be able to conclude about the solidification cracking susceptibility from the crack lengths of different Vastrestraint specimens, the loading time induced portion d_{def} caused by the duration of the deformation t_{def} must therefore be taken into account.

In case of a centerline crack propagating in welding direction, the portion d_{def} is equal to d_{SF} which is the distance that the weld pool moves with a travel speed v_s during the deformation time t_{def} (Equation (5)), as illustrated in Figure 4.

$$d_{\text{def}} = d_{\text{SF}} = v_s \cdot t_{\text{def}} \quad (5)$$

Centerline cracks are a special case. Solidification cracks that develop as a result of MVT testing are typically distributed in the weld metal (see Figure 3). Nevertheless, the propagation of these cracks mostly occurs along the preferred direction of crystallization, and thus approximately perpendicular to the melt pool isotherms, i.e. the liquidus isotherm. Due to the elliptical shape of the isotherms, their distance - and thus the maximum possible crack length - decreases with increasing distance from the center of the weld, as shown in Figure 4. The maximum crack length typically appears in the centerline, while cracks near the fusion line are shortest.

Cracks do not necessarily grow to their maximum possible length (saturated cracks). They may stop before the end of deformation has reached. On the other hand, cracks may propagate further beyond the deformation time. Therefore, a simple subdivision of the crack lengths into d_{BTR} and d_{def} from the crack appearance alone is not possible. The amount of both parts remains unknown. However, a saturation factor f_s can be calculated (Equation (6)). This allows for a reliable statement as to whether the growth of the crack with the length L exceeds or falls below the deformation limit d_{def} .

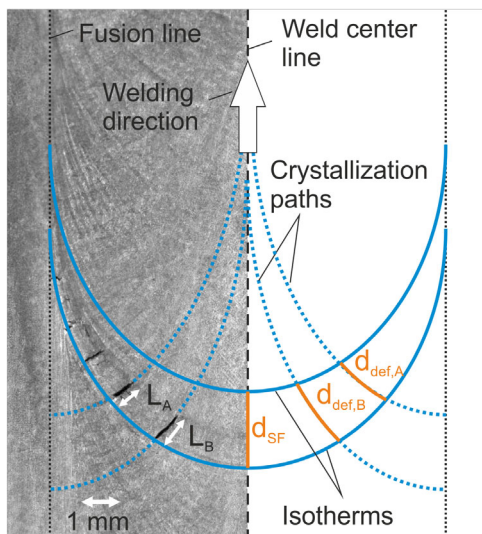


Figure 4. Crack propagation along crystallization paths depending on the location in the weld metal. L_A and L_B are exemplary crack lengths. The individual distances d_{SF} , $d_{\text{def,A}}$ and $d_{\text{def,B}}$ are determined by the displacement of the isotherms by the welding speed during loading, martensitic filler material, 4% bending strain.

$$f_s = \frac{L}{d_{\text{def}}} \quad (6)$$

As soon as several cracks appear on the specimen, an evaluation must consider the totality of the cracks. The standard MVT evaluation procedure uses the total crack length TCL for this purpose. Similarly, a saturation factor can be applied to the totality of all cracks in a specimen. However, since this is a relative value, no sum can be formed as in the case of TCL, but an average value must be found. For this purpose, the relative crack length RCL is defined as the arithmetic mean of the saturation f_s of all cracks (number n) in the specimen according to Equation (7).

$$\text{RCL} = \frac{\sum_{i=1}^n f_s}{n} \quad (7)$$

The saturation factor RCL serves as a material-specific parameter that can be used to determine the load induced cracking susceptibility under certain welding conditions. The following cases are to be distinguished.

RCL = 0, noncritical range

No cracking occurs.

$0 < \text{RCL} < 1$, subcritical range

Cracks are formed but stay in average shorter than deformation allows. Crack growth is delayed or stopped before the end of the deformation. The material is prone to cracking under the welding conditions applied, but the loading time induced cracking susceptibility is low.

RCL ≥ 1 , critical range

Cracks occur and grow as long as the deformation lasts (RCL = 1, saturation limit) or even longer. This means welding conditions where the material is highly susceptible to a loading time induced cracking.

In contrast to the determination of the TCL, the respective fraction d_{def} necessary to calculate RCL must be determined separately for each crack as a function of the crack location along the isotherms. For this purpose, an image-based numerical approach is followed.

As illustrated in Figure 4, by identifying the initiation point of a crack its ideal crystallization path is assumed orthonormal to the isotherm at this location. The crack propagation d_{def} along this path during the deformation time t_{def} is calculated numerically.

First, an isotherm (along the melt pool radius) is manually defined from a surface image of a sample based on, for example, ripple lines or the shape of the end crater. The lateral boundary results from the melt line (cf. Figure 4). The isotherm is described mathematically by an ellipse according to Equation (8), as shown in Figure 5.

$$f(x) = \frac{a}{b} \cdot \sqrt{b^2 - x^2} \quad (8)$$

The crystallization path $c(x)$ can be described using a finite number of linear segments s_n . In Figure 5, for reasons of clarity, only the subdivision into three segments is shown. In the actual calculation a number of at least 100 segments is used. The calculation is carried out numerically, to be able to model also melt pools, which cannot be described mathematically by an ellipse. The proportions x_n and y_n of the

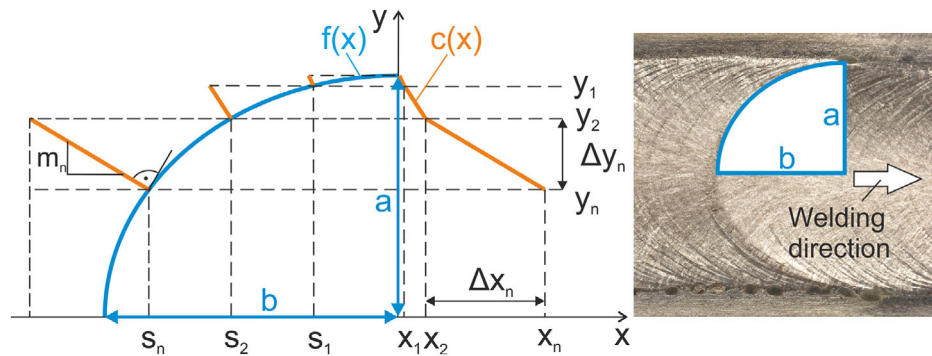


Figure 5. Schematic of the determination of the crystallization path $c(x)$ by subdividing it into a number of n linear paths. The ellipsoid $f(x)$ represents the border of the melt pool, i. e. the liquidus isotherm.

Table 1. Chemical compositions of welding consumables in wt%.

Alloy	C	Cr	Mn	Ni	Si	Fe
CrMn	0.07	10.34	9.45	0.38	0.38	Bal.
CrNi	0.07	7.41	0.49	6.08	0.27	Bal.

crystallization path $c(x)$ are calculated according to Equation (9) and (10).

$$x_n = (f(s_{n-1}) - f(s_n)) \cdot f'(s_n) + x_{n-1} \quad (9)$$

$$y_n = f(s_n) \quad (10)$$

For each crack whose start coordinates are measured, its theoretically expected length d_{def} can be obtained along the numerically calculated crystallization path $c(x)$ and compared to the actual crack length. By applying this to all cracks found in the weld metal, the saturation f_s and therefore the relative crack length RCL can be determined. In the following, a comparison is made between the conventional evaluation based on TCL and the newly developed evaluation using RCL.

4. Experimental Section

4.1. Materials

Two high-alloyed martensitic welding consumables were investigated regarding their solidification cracking susceptibility in the MVT test. In both cases, these are experimental batches of commercially unavailable flux-cored filler wires of so-called Low Transformation Temperature (LTT) alloys, which are used

for residual stress control during welding of high-strength steels.^[43,44] For this purpose, the low martensite start temperature of the materials is exploited, which is, however, not of importance for the present hot cracking investigations. The chemical compositions of the materials designated in the following as CrMn and CrNi are shown in **Table 1**.

4.2. Welding and MVT Test

Both filler metals were first welded in five beads in preconditioned grooves of specimens made of the high-strength low-alloy steel S960Q (minimum yield strength 960 MPa). Argon with 8% CO₂ addition was used as shielding gas. The welding speed was kept constant at 5.8 mm s⁻¹ for all beads, with an energy input per unit length of 9 kJ cm⁻¹. The specimens were then milled and ground to final dimensions (length × width × height) for MVT testing of 100 × 40 × 10 mm. The MVT test was performed using the parameters listed in **Table 2** as usual GTAW remelts. Heat input per unit length and welding speed were varied. The strain rate was adjusted in three steps in each case. It was calculated based on the augmented strain and the deformation time following Equation (2). The tests were repeated three times. The evaluation was then performed as described in Section 2 and 3.

5. Results

5.1. Conventional Evaluation

Figure 6 shows the conventionally determined TCL of the material CrMn as a function of strain rate for different welding parameter combinations. A clear dependence on the strain rate cannot be quantified. For higher heat input (14 kJ cm⁻¹), the

Table 2. Parameters used for MVT test.

Parameter set	Energy input per unit length E [kJ cm ⁻¹]	Welding speed v_s [mm s ⁻¹]	Welding current [A]	Augmented strain ϵ [%]	Strain rate $\dot{\epsilon}$ [s ⁻¹]	Welding voltage [V]
7.6-3	7.6	3	190	4	0.07; 0.21; 0.63	12
7.6-1.8	7.6	1.8	114	4	0.07; 0.21; 0.63	12
14-1.8	14	1.8	210	4	0.07; 0.21; 0.63	12

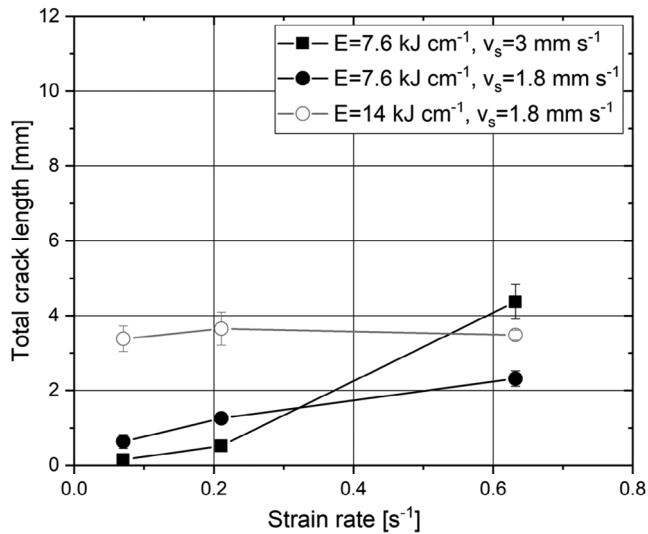


Figure 6. Total crack length (TCL) as function of the strain rate for alloy CrMn depending on the welding parameters (heat input E and welding speed v_s).

crack length remains approximately constant, while it tends to increase for the lower heat input (7.6 kJ cm^{-1}). The increase in crack length with strain rate at fast welding speed (3 mm s^{-1}) is more pronounced.

The total crack lengths of the CrNi material are higher compared to the manganese-alloyed material for all welding parameter sets (Figure 7). Here, the longest cracks occur at the highest heat input, too. In contrast, there is no significant dependence on the welding speed. It is not intuitive that the crack length decreases in each case with increasing strain rate, as a material's cracking susceptibility is expected to increase with higher strain rates. The scatter of crack lengths is higher at lower strain rates.

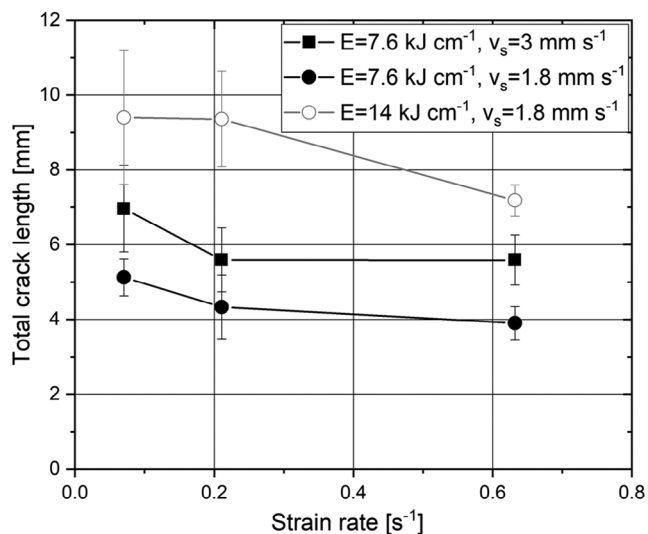


Figure 7. Total crack length (TCL) as function of the strain rate for alloy CrNi depending on the welding parameters (heat input E and welding speed v_s).

The conventional evaluation based on the TCL shows that CrNi is more susceptible to solidification cracking than CrMn. Higher heat input per unit length tends to be more critical for crack formation. The influence of the welding speed is not clear. Hence, a classification of the individual parameter sets is not possible based on TCL. As a result, both materials would be conventionally classified as “hot crack resistant” (TCL < 15 mm, at 4% augmented strain) for all parameter sets according to the classical evaluation approach.

5.2. New Evaluation

The results of the evaluation based on the relative crack length RCL for the material CrMn are shown in Figure 8. For all parameter sets, there is an almost linear increase in RCL with the strain rate. The highest heat input leads to the highest relative crack lengths. The slow welding speed shows the lowest crack occurrence. The saturation limit of RCL = 1 or 100% is exceeded only at the highest strain rate. This means that for low strain rates, crack growth is stopped before the end of the mechanical loading is reached.

The material CrNi also shows the almost linear dependence of RCL on the strain rate (Figure 9). However, the strain-related increases are more pronounced here. For the slow welding speeds, the saturation limit of 100 % is already reached at a strain rate just above 2 s^{-1} . At the highest strain rate, the relative crack length is approximately doubled compared to the saturation limit at the lower heat input. With increasing strain rate, the high heat input leads to a strong crack length increase far beyond the saturation limit. On average, a relative crack length of 450% is reached. Compared to the conventional evaluation, which is not able to represent this dependence, a clear differentiation between the parameter sets is made possible.

In order to establish a single characteristic value for the respective parameter sets, the available database can be used

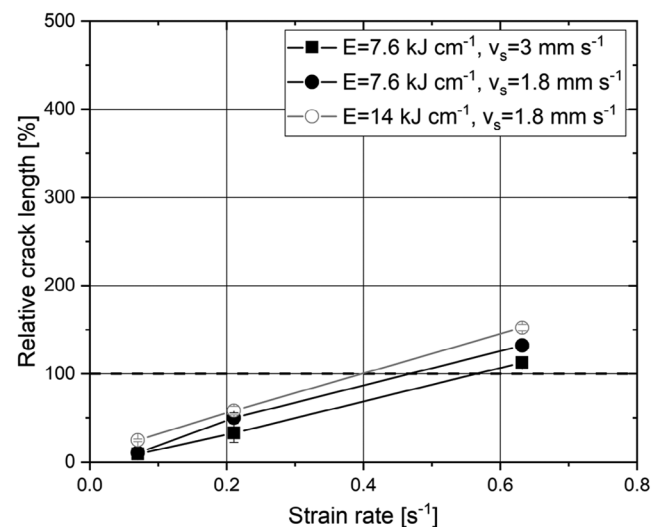


Figure 8. Relative crack length (RCL) as function of the strain rate for alloy CrMn depending on the welding parameters (heat input E and welding speed v_s), saturation limit indicated by dashed line.

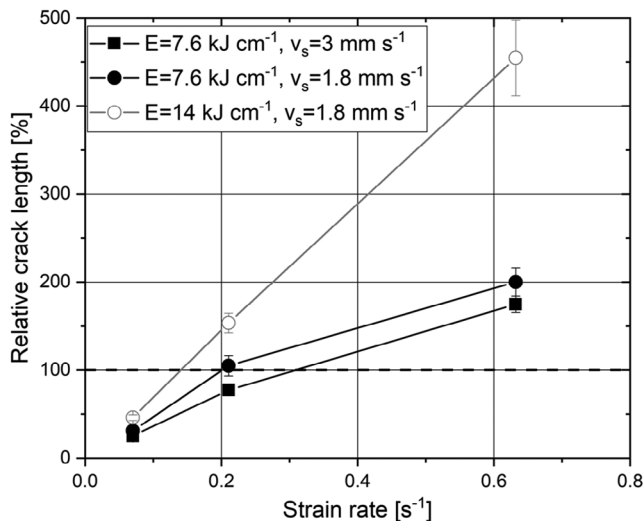


Figure 9. Relative crack length (RCL) as function of the strain rate for alloy CrNi depending on the welding parameters (heat input E and welding speed v_s), saturation limit indicated by dashed line.

to estimate a critical strain rate at which complete saturation of the crack length is to be expected. This is significant in that it represents the limit above which the material (with a given parameter set) shows increasing sensitivity to mechanical loading. Below this value, cracking appears possible, but is less load dependent. To determine the critical strain rate, the individual RCL curves were fitted linearly as a function of strain rate. The critical strain rate as intersection at $RCL = 100\%$ is shown in **Figure 10** for the individual parameter sets.

It is clear from **Figure 10** that the welding parameters have the same effect on the cracking behavior of both materials. This could not be deduced from the conventional evaluation. Slower welding speed with higher heat input increases the cracking tendency. The smaller the value of the critical strain rate, the higher the cracking potential.

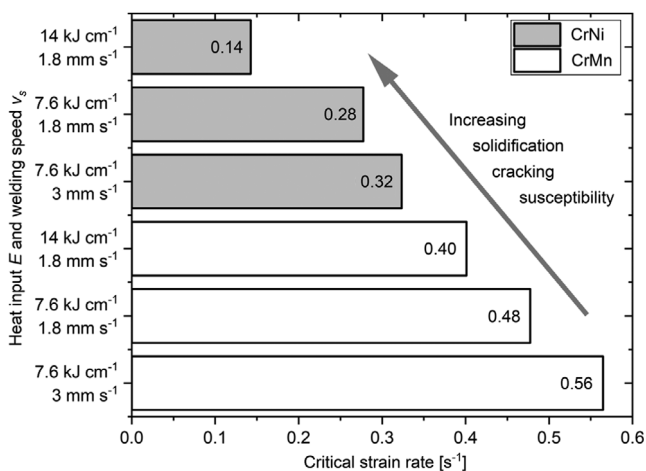


Figure 10. Critical strain rate for different sets of welding parameters of the alloys CrNi and CrMn.

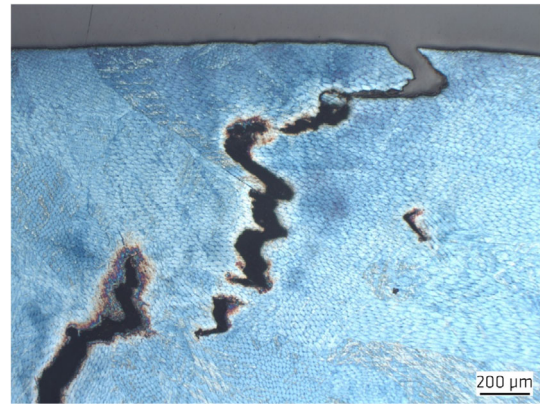


Figure 11. Solidification cracks and cellular structure in the cross-sections of the CrNi alloy (etchant LB I) $E = 14 \text{ kJ cm}^{-1}$, $v_s = 1.8 \text{ mm s}^{-1}$.

The higher cracking susceptibility of the material CrNi compared to CrMn, is also supported by the microstructure. **Figure 11** shows the etched microstructure in the cross-section of the alloy CrNi. A coarse cellular structure is apparent. This is an indication of a primary austenitic solidification accompanied by an unfavorable segregation profile, which tends to result in a higher risk of solidification cracking. The cracks open quite broadly and extend below the surface. In contrast, the CrMn alloy shown in **Figure 12** does not show a pronounced cell structure. Nevertheless, cracks are clearly visible, which have probably healed due to backfilling indicated by the light-colored filling. We assume that this behavior, which is also known from nickel-based materials, helps the material to achieve a higher hot cracking resistance. The cracks also appear finer, but also continue to spread below the surface of the material. Further investigations are necessary to clarify the causes.

The results obtained are consistent with the solidification cracking model according to Prokhorov, who postulates a temperature and load dependent critical strain rate necessary to initiate cracking. The new strain rate-based evaluation of the relative crack length RCL in the MVT test thus allows for practical assessment of the solidification cracking susceptibility



Figure 12. Solidification cracks and indicated backfilling in the cross-sections of the CrMn alloy (etchant LB I + 2% Nital) $E = 14 \text{ kJ cm}^{-1}$, $v_s = 1.8 \text{ mm s}^{-1}$.

of a material considering welding as well as mechanical parameters. The general applicability of the new evaluation method must be validated based on further materials and tests. In particular, nickel-based alloys, austenitic steels and aluminum alloys, which are most susceptible to hot cracking, are to be tested. The next step could be an international round robin test to compare the results of different Vareststraint test machines. In further research, the surface-based concept should also be extended to the volume of the weld metal. We have already shown promising approaches here using computer tomography (CT).^[45] From this, even more information can be obtained regarding the crack-critical load.

6. Conclusion

A new image-based evaluation methodology allows the loading time-related portion of the crack length to be assessed as a function of crack location for Vareststraint tests. Influences of the welding parameters can thus be clearly quantified based on the strain rate. The approach was demonstrated using two martensitic filler metals, for which the following conclusions can be drawn: 1) The cracking susceptibility increases linearly with higher strain rates for all parameter sets. 2) The Ni-alloyed filler shows the higher cracking susceptibility compared to the Mn-alloyed one. 3) Higher heat input at slower welding speeds consistently leads to higher crack formation for both materials. 4) The plot of the relative crack length RCL as a function of the strain rate allows the identification of a critical strain rate as a characteristic value of the solidification cracking susceptibility for a given set of welding parameters.

Acknowledgements

This research was funded by German Research Foundation (DFG) grant number KR3917/2-2, KA1807/9-1 and GI376/8-1.

Open Access funding enabled and organized by Projekt DEAL.

Conflict of Interest

The authors declare no conflict of interest.

Data Availability Statement

The data that support the findings of this study are available from the corresponding author upon reasonable request.

Keywords

low transformation temperature alloys, solidification cracking, vareststraint test, welding

Received: November 30, 2021

Revised: March 3, 2022

Published online:

- [1] B. Hemsworth, T. Boniszewski, N. F. Eaton, *Met. Constr.* **1969**, 1.
[2] ISO 17641-1:2004, *Destructive tests on welds in metallic materials - Hot cracking tests for weldments - Arc welding processes - Part 1: General.*

- [3] C. E. Cross, in *Hot Cracking Phenomena In Welds*, (Eds: T. Böllinghaus, H. Herold), Springer, Berlin, Heidelberg, New York, **2005**.
[4] N. Coniglio, C. E. Cross, *Int. J. Adv. Manuf. Technol.* **2020**, 107, 5011.
[5] J. C. Lippold, *Welding Metallurgy and Weldability*, John Wiley & Sons, Inc., Hoboken, NJ, USA **2015**.
[6] W. R. Apblett, W. S. Pellini, *Welding J.* **1954**, 2, 83.
[7] J. C. Borland, *Br. Welding J.* **1960**, 7, 508.
[8] F. Matsuda, H. Nakagawa, K. Sorada, *Trans. JWRI* **1982**, 11, 67.
[9] F. Matsuda, *Proc. 1st US-Japan Symp. on Advances in Welding Metallurgy*, American Welding Society, San Francisco **1990**.
[10] M. Rappaz, J. M. Drezet, M. Gremaud, *Metall. Mater. Trans.* **1999**, 30A, 449.
[11] P. Yu, K. J. Thompson, J. McCarthy, S. Kou, *Welding J.*, **2018**, 97, 301s.
[12] S. Kou, *Acta Mater.* **2015**, 88, 366.
[13] S. Kou, *Welding J.* **2015**, 94, 374.
[14] S. Kou, *Metals* **2021**, 11, 1442.
[15] Y. Zhang, X. Xu, *Metall. Mater. Trans. A* **2021**, 52, 985.
[16] N. N. Prokhorov, N. Nikol, *Prokhorov, Trans. Jpn. Welding Soc.* **1971**, 2, 109.
[17] T. Senda, F. Matsuda, G. Takano, K. Watanabe, T. Kobayashi, T. Matsuzaka, *Trans. Jpn. Welding Soc.* **1971**, 2, 45.
[18] F. Matsuda, H. Nakagawa, K. Nakata, H. Kohmoto, Y. Honda, *Trans. JWRI* **1983**, 12, 65.
[19] F. Matsuda, H. Nakagawa, H. Kohmoto, Y. Honda, Y. Matsubara, *Trans. JWRI* **1983**, 12, 73.
[20] F. Matsuda, H. Nakagawa, S. Tomita, *Trans. JWRI* **1986**, 15, 125.
[21] D. Abe, F. Matsuzaka, Y. Murakami, T. Matsuoka, H. Yamaoka, *Weld. World* **2018**, 62, 1237.
[22] N. Coniglio, C. E. Cross, *Int. Mater. Rev.* **2013**, 58, 375.
[23] K. Nakata, F. Matsuda, *Trans. Jpn. Welding Soc.* **1995**, 24, 83.
[24] T. Kannengiesser, T. Boellinghaus, *Weld. World* **2014**, 58, 397.
[25] ISO 17641-2:2015 *Destructive tests on welds in metallic materials - Hot cracking tests for weldments - Arc welding processes - Part 2: Self-restraint tests.*
[26] ISO/TR 17641-3:2005 *Destructive tests on welds in metallic materials - Hot cracking tests for weldments - Arc welding processes - Part 3: Externally loaded tests.*
[27] S. Yamashita, S. Okano, M. Mochizuki, K. Saida, *Weld. World* **2021**, 65, 2013.
[28] C. Gollnow, T. Kannengiesser, *Weld. World* **2013**, 57, 277.
[29] N. Bakir, V. Pavlov, S. Zavjalov, S. Volvenko, A. Gumenyuk, M. Rethmeier, *Weld. World* **2018**, 63, 435.
[30] H. E. Coules, P. Colegrove, L. D. Cozzolino, S. W. Wen, *J. Mater. Process. Technol.* **2012**, 212, 962.
[31] H. Herold, M. Streitenberger, A. Pchennikov, in *Mathematical Modelling Of Weld Phenomena 5* (Eds: H. H. Cerjak, H. K. D. H. Bhadeshia), IOM Communications, Institute of Materials, London, Book **2001**, p. 738.
[32] F. Matsuda, H. Nakagawa, K. Nakata, H. Okada, *Trans. JWRI* **1979**, 8, 85.
[33] K. U. N. Liu, P. Yu, S. Kou, *Welding J.* **2020**, 99, 255s.
[34] W. F. Savage, C. D. Lundin, *Welding J.* **1965**, 44, 433s.
[35] M. Thomas, J. Vollert, J. Weidemann, J. Gibmeier, A. Kromm, T. Kannengiesser, *Weld. World* **2020**, 64, 913.
[36] D. Statharas, H. Atkinson, R. Thornton, J. Marsden, H. B. Dong, S. W. Wen, *Metall. Mater. Trans. A: Phys. Metall. Mater. Sci.* **2019**, 50a, 1748.
[37] AWS (2016): *ANSI AWS B4.0:2016: Standard Method for Mechanical Testing of Welds.*

- [38] K. Wilken, H. Kleistner, *Mater. Tech.* **1982**, *1*, 3.
- [39] G. E. Santos, É.M. Miná, D. A. C. Pequeno, H. C. de Miranda, C. C. Silva, *Weld. World* **2021**, *65*, 1969.
- [40] V. Shankar, T. P. S. Gill, S. L. Mannan, S. Sundaresan, *Sci. Technol. Weld. Joining* **2013**, *5*, 91.
- [41] M. M. Johansson, P. Stenvall, L. Karlsson, J. Andersson, *Weld. World* **2020**, *64*, 903.
- [42] N. Coniglio, C. E. Cross, in *Hot Cracking Phenomena In Welds IV* (Eds: T. Böllinghaus, J. C. Lippold, C. E. Cross), Springer International Publishing, Switzerland, **2016**.
- [43] S. W. Ooi, J. E. Garnham, T. I. Ramjaun, *Mater. Des.* **2014**, *56*, 773.
- [44] A. Kromm, J. Dixneit, T. Kannengiesser, *Weld. World* **2014**, *58*, 729.
- [45] F. Vollert, M. Thomas, A. Kromm, J. Gibmeier, *Materials* **2020**, *13*, 2726.